Biomaterials 34 (2013) 4703–4713

Contents lists available at SciVerse ScienceDirect

Biomaterials

journal homepage: www.elsevier.com/locate/biomaterials

The impact of chronic blood–brain barrier breach on intracortical electrode function

Tarun Saxena [1], Lohitash Karumbaiah [1], Eric A. Gaupp, Radhika Patkar, Ketki Patil, Martha Betancur, Garrett B. Stanley, Ravi V. Bellamkonda*

Wallace H. Coulter Department of Biomedical Engineering at Georgia Institute of Technology, Emory University School of Medicine, Atlanta, GA 30332, USA

ARTICLE INFO

Article history:
Received 16 February 2013
Accepted 3 March 2013
Available online 2 April 2013

Keywords:
Brain
Electrode
Inflammation
Foreign body response
Blood

ABSTRACT

Brain-computer interfaces (BCIs) have allowed control of prosthetic limbs in paralyzed patients. Unfortunately, the electrodes of the BCI that interface with the brain only function for a short period of time before the signal quality on these electrodes becomes substantially diminished. To truly realize the potential of BCIs, it is imperative to have electrodes that function chronically. In order to elucidate the physiological determinants of a chronically functional neural interface, we studied the role of the blood–brain barrier (BBB) in electrode function, because it is a key mediator of neuronal hemostasis. We monitored the status of the BBB and the consequences of BBB breach on electrode function using non-invasive imaging, electrophysiology, genomic, and histological analyses. Rats implanted with commercially available intracortical electrodes demonstrated an inverse correlation between electrode performance and BBB breach over a period of 16 weeks. Genomic analysis showed that chronically functional electrodes elicit an enhanced wound healing response. Conversely, in poorly functioning electrodes, chronic BBB breach led to local accumulation of neurotoxic factors and an influx of pro-inflammatory myeloid cells, which negatively affect neuronal health. These findings were further verified in a subset of electrodes with graded electrophysiological performance. In this study, we determine the mechanistic link between intracortical electrode function and failure. Our results indicate that BBB status is a critical physiological determinant of intracortical electrode function and can inform future electrode design and biochemical intervention strategies to enhance the functional longevity of BCIs.

1. Introduction

The field of human brain–computer interface (BCI) research is rapidly progressing [1,2]. Intracortical interfaces hold the promise of enabling single/multi-unit recordings that are capable of controlling a range of neuroprosthetics including those designed for amputees or stroke patients [3–6]. However, long-term recording from intracortical electrodes remains a challenge, in part due to an adverse tissue response at the brain–electrode interface. This deleterious response results in decreased neuronal viability, and the formation of a glial capsule around the implant [7]. While the glial response has been well characterized, the mechanistic link between the physiological events at the brain–electrode interface and chronic electrode performance is missing. This is important because there exists a temporal disconnect as the scar stabilizes well before the onset of recording failure. In order to design electrodes that preserve recording function over the long-term, it is critical to uncover the mechanisms governing electrode compatibility, neuronal health, and recording success. As blood–brain barrier (BBB) disruption underlies many neurodegenerative neuropathologies [8], we investigated the contribution of BBB breach and consequent infiltration of neurotoxic factors and pro-inflammatory myeloid cells to neuronal health [9,10] and the failure of chronically implanted intracortical electrodes.

In this study, we hypothesized that chronic BBB breach is a key determinant of electrode failure. To test this hypothesis, we implanted adult rats with two widely used commercially available Michigan (planar) and microwire (microarray) intracortical electrode arrays [7] and correlated their performance to a quantitative analysis of BBB breach and subsequent infiltration of myeloid cells and neurotoxic factors. Using quantitative non-invasive imaging, immunohistological methods, and genomic approaches, we

* Corresponding author. Wallace H Coulter Department of Biomedical Engineering, 313 Ferst Drive, Atlanta, GA 30332-0535, USA. Tel.: +1 404 385 5038; fax: +1 404 385 5044.
E-mail addresses: ravi@gatech.edu, ravi@bme.gatech.edu (R.V. Bellamkonda).
[1] These authors contributed equally to this work.

0142-9612/$ – see front matter © 2013 Elsevier Ltd. All rights reserved.
http://dx.doi.org/10.1016/j.biomaterials.2013.03.007

assessed the chronic sequelae of an electrode-related cortical insult. Additionally, we also evaluated if electrode performance and BBB breach are graded and correlated by quantifying the wound healing response as characterized by the presence of proteins that are anti-inflammatory or contribute to maintaining the integrity of the BBB. Finally, we tested the hypothesis that BBB breach can explain variability in performance within electrodes of the same physical design (microwire). In this study we: a) quantitatively investigate the state of the BBB around intracortical electrode implants and its contribution in determining the performance of chronically implanted intracortical electrodes; and b) evaluate a preclinical imaging modality to non-invasively monitor the state of the BBB around intracortical electrodes.

2. Materials and methods

2.1. Surgical procedures and electrode implantation

All animal procedures were approved by the Institutional Animal Care and Use Committees (IACUC) at Georgia Institute of Technology. A total of fifty-six (56) adult male Sprague Dawley rats (10–12 weeks old, ~250 gm) were implanted with electrodes and allowed to survive for 3 days or 16 weeks post-implantation (16WPI). Eight (8) animals were used for electrophysiological recordings ($n = 4$/electrode type); 28 animals were used for non-invasive BBB monitoring ($n = 4$/electrode type, 4 naïve animals and 4 sham animals); and 20 animals were used for genomic and histological analysis. For each of these procedures a single adult male was anesthetized using 2% isofluorane and its head depilated. The animal was transferred to a stereotaxic frame (David Kopf Instruments, CA) fitted with a nose/tooth bar assembly and an anesthesia mask to deliver isofluorane continuously. The animal's body temperature was regulated via feedback controlled heating and heart-rate and respiration monitored throughout the procedure. Lidocaine was injected subdermally as a local anesthetic, following which a single midline incision was made. The skin flaps were retracted and held down by hemostatic clamps to expose the skull, the periosteum scraped away and the skull surface cleaned using a Q-tip soaked in 3% hydrogen peroxide. A craniotomy was made ~1.5 mm posterior from anterior bregma and ~4 mm lateral from the midline, followed by the placement of four bone screws, 2 anterior to bregma and 2 posterior to lambda. The dura-mater was subsequently removed and either a Microwire electrode array (50 μm diameter, TDT, FL) or Michigan electrode array (50 μm thick, Neuronexus, MI) was stereotaxically implanted to a depths of ~800 μm and 1200 μm in the rat barrel cortex respectively. The craniotomy was covered with sterile 2% SeaKem agarose (Lonza, NJ) and sealed with UV curing dental cement which was also used to build the head cap. The hemostats were subsequently removed and the skin flap sutured back. The animal was injected with buprenorphine HCl and allowed to recover before returning it to the cage. All procedures were the same for the cytokine/histology group and non-invasive imaging group except that they were implanted with dummy electrodes and the non-invasive imaging group was not headcapped with bone cement. Sham animals received a craniotomy followed by a durotomy, but no electrode implant.

2.2. Brain tissue preparation and immunohistochemistry

3 days and 16 weeks post electrode implantation, animals were transcardially perfused with PBS, followed by 4% paraformaldehyde, followed by 30% sucrose in PBS (300 ml each) and brain tissue for immunohistochemical analysis ($n = 6$/electrode type) was sectioned as described previously [11]. For LCM, the electrodes were gently extracted after soaking overnight at 4 °C in 30% sucrose in PBS, and the brains were snap frozen and stored at −80 °C. Brain tissue was sectioned at a thickness of 15 μm using a cryostat, and serial sections were collected on polyethylene naphthalate (PEN) membrane slides (Life Technologies, NY) for LCM, and on charged glass slides (VWR, PA) for immunohistochemical analysis. The sections were subsequently incubated overnight with the appropriate primary antibody (Table S1). Following primary antibody incubation, the sections were washed thrice with PBS and subsequently blocked with blocking buffer (PBS containing 4% goat serum and 0.5% Triton-X100) for 1 h. Sections were then incubated for 1 h with blocking buffer containing 1:220 dilutions of appropriate secondary antibodies (Table S1). Following secondary antibody incubation, sections were washed several times with PBS, stained for 15 min with 4′,6-diamidino-2-phenylindole (DAPI) nuclear stain (Life Technologies, NY), and coverslipped after three washes with PBS using Fluormount-G (Southern Biotech, AL). Sections were stored at −20 °C until imaged. For chromogenic stains (AT-8 and PHF), sections were stained using a diaminobenzidine (DAB) histochemistry kit (Molecular Probes, OR) according to protocols provided by the manufacturer. Tissue sections were imaged on a Zeiss Axiovert 200M (Carl Zeiss, NY) using equal exposure times for fluorescent markers across 3 Day and 16 week tissue sections. The exposure times were set below saturation of the digital camera.

2.3. Quantification of immunofluorescence

Five sections (per animal) spanning the depth of the electrode were imaged for quantification to investigate the response at different depths in the cortical column. Fluorescent intensity as a function of distance from the electrode–tissue interface was calculated for IgG and Albumin stained sections using MATLAB (with Image Processing Toolbox, Mathworks, MA), as previously described [9,12].

2.4. Laser capture microdissection

PEN membrane slides containing brain tissue sections for LCM were placed on a cold block and fixed for 2 min in ice-cold 75% ethanol, followed by three rinses of PBS prepared with ice-cold nuclease free water (Qiagen, CA). Sections were then stained for 1 h with 1:220 dilution of goat anti-rat IgG + 500 U RNase inhibitor (Life Technologies, NY). The sections were rinsed thrice with nuclease free PBS and subsequently serially dehydrated with 75%, 95% and 100% ethanol for 15 s each. Sections were allowed to air dry for 5 min on the ice block before proceeding directly to LCM. PEN membrane slides containing IgG stained 3 day and 16 week tissue sections were laser capture micro-dissected using an Arcturus XT Laser Capture Microdissection System (Life Technologies, NY), as described previously [11].

2.5. qRT-PCR array analysis

Tissue sections from multiple 3 day, 16 week and naïve ($n = 4$/group) animals, and from MWA3 and MWA5 were laser capture microdissected. To probe the abundance of transcripts encoding various myeloid cells activating, BBB regulating cytokines and matrix metalloproteinases (Table 1), RNA extraction, quantification, and gene expression assays were run according to methods previously described [11]. Expression data was normalized against the average expression of two endogenous housekeeping genes–GAPDH and HPRT. The ratio of treatment to control sample normalized target mRNA expression was analyzed by Student's *t*-test.

2.6. Synthesis of fluorochrome (Albumin-Cy7) to assess BBB breach

Amine reactive Cy7, near-infrared (NIR) fluorescent dye (Cy7-NHS ester, Lumiprobe Corp.,FL, excitation/emission 745/780 nm) was conjugated to bovine serum albumin (BSA, Sigma A9418) according to manufacturer's protocols, and yielded ~ 4 Cy7 molecules per albumin. The protein concentrations of Albumin-Cy7 was determined with a Bradford's assay [13] by measuring the absorption at 595 nm with a UV-Vis system using standard solutions of known concentrations of BSA. The fluorophore concentration was determined using standard curves for Cy7 and measuring the fluorescence of Albumin-Cy7 at 745 nm with a multispectral plate reader (Biotek, VT).

2.7. In vivo fluorescence molecular tomography (FMT) to assess BBB breach

Immediately prior to *in vivo* imaging, a bolus intravenous (i.v.) injection of Albumin-Cy7 (15 nmoles in PBS, 1 ml total volume) was administered via the tail vein. For *in vivo* imaging, rats were anesthetized by gas anesthesia (isoflurane/oxygen mixture), placed in a FMT4000 system (Perkin Elmer, MA) imaging chamber one at a time and imaged. Additionally, each animal's head was shaved and a depilatory cream applied to ensure good coupling between the laser and tissue. The FMT works in transillumination mode and a laser (750 nm) scans the surface of the animal in a user defined grid. The system automatically adjusts exposure time and laser power to avoid saturation and reduce noise. The fluorescence is detected by a charge-coupled device detector on the opposite side. Total scan times are around 5 min. Three-dimensional

Table 1
Transcript levels of neurotoxic and myeloid cell regulating cytokines in best (MWA5) and worst (MWA3) performing microwire implanted animals. Data are represented as mean ± 1 SD ($n = 3$ measurements/gene transcript).

Gene	MWA3	MWA5
Myeloid cell regulating cytokines		
IL12β	16.52 ± 0.13	–
TNFsF13B	160.53 ± 12.79	143.14 ± 4.61
IL17α	34.23 ± 5.4	6.5 ± 0.32
IFNγ	–	–
Neurotoxic Cytokines		
IL1β	60.95 ± 0.04	42.34 ± 0.84
TNFα	7.05 ± 0.12	5.79 ± 1.14
IL-6	16.08 ± 4.1	–
IL1Ra	15.5 ± 1.18	34.49 ± 3

ROIs were drawn around implant and stab regions and the total amount of fluorochrome were calculated using the FMT software (TrueQuant 3). Data were normalized to sham injured animals, to account for any changes due to surgical procedures.

2.8. Electrophysiological recordings

Single-unit extracellular recordings were collected using a 32-channel data-acquisition system (Plexon Inc., TX). Neuronal signals were amplified, band-pass filtered (500–5000 Hz), and digitized at 40 kHz/channel. Recordings were analyzed using the OfflineSorter software suite (Plexon Inc., TX) to assign the recorded spike waveforms to single-units on the basis of standard template matching techniques and physiologically plausible refractory periods. All cortical cells were located at stereotaxic depths of 500–900 μm, presumably within cortical layer IV of the rat barrel cortex. Cortical cells were classified as spiking units based on the width of action potential waveform. A recorded neuron was classified as a spiking unit when the initial trough was >200 μs and the total duration of the waveform was >1200 μs, and the spontaneous firing rate < 1 Hz. Following this classification, only spiking units were recorded in the subsequent whisker stimulations. The signal to noise ratio (SNR) was computed using a custom Matlab script according to the following equation:

$$\mathrm{SNR} = \left(\frac{\text{Amplitude of max[peak, trough] of spike waveform}}{3^{*}\text{Standard Deviation of Noise}}\right)^{2}$$

An SNR of 1.25 was set as the threshold and any value at or below 1.25 was considered noise.

2.9. Statistical analysis

All statistical inferences for FMT data and immunofluorescence quantification were made between differing time points using a Student's *t*-test. Student's *t*-tests were performed after ascertaining equal or unequal variances using an F-test. For all tests, $p < 0.05$ was considered significant. For the gene expression data, a greater than three-fold (±3) change was considered significant [11].

3. Results

3.1. Degree of BBB breach across electrode types

In order to non-invasively assess the state of the BBB around intracortical electrode implants, animals were administered equal intravenous doses (15 nmoles) of Albumin-Cy7 and accumulation of the fluorophore around electrode implant sites in the barrel cortex was quantified using fluorescence molecular tomography (FMT). Albumin extravasation is a well-established indicator of compromised BBB in a variety of pathophysiological conditions

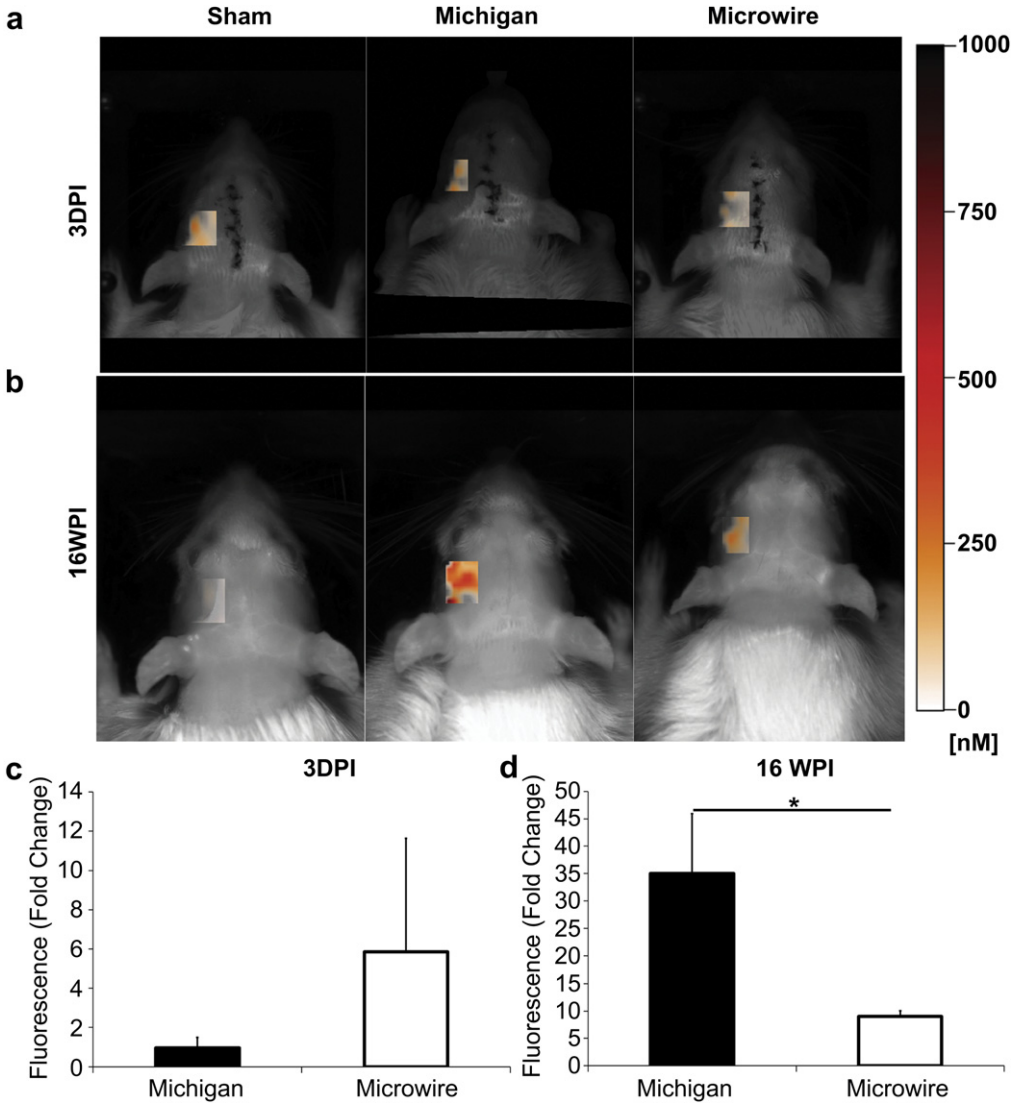

Fig. 1. Non-invasive assessment of BBB breach. From left to right, the left panel is sham animals, the middle panel is Michigan electrode implanted animals, and the right panel is representative of microwire electrode implanted animals. (a) Accumulation of albumin-Cy7 around implant sites at 3DPI which is quantified in (c). (b) Accumulation of albumin-Cy7 around implant sites at 16WPI which is quantified in (d). In Fig. 2c and d, data are normalized to sham animals. Values are represented as mean ± s.e.m ($n = 4$/group).

[14–17]. In order to account for variations arising due to surgical procedures, data were normalized to age-matched sham animals that received a craniotomy and durotomy, but no electrode implant. Results from the FMT imaging at three days post-implantation (3DPI - Fig. 1a,c), indicated no significant differences between the Michigan and microwire electrode implanted animals, possibly due to edema at acute stages of injury [18]. However, at 16WPI (Fig. 1b,d, Fig. S1, Movie S1), significant differences were observed between implant groups. The Michigan electrodes exhibited a significantly higher breach in comparison to the microwire electrodes ($p < 0.01$). FMT imaging based BBB quantification was validated by immunohistochemical staining of tissue sections with antibodies against the rat serum proteins albumin and IgG. The fluorescence intensity, as a function of distance from shank sites, was quantified and integrated [9,12]. Immunoreactivity for the rat serum proteins, albumin (Fig. 2a,b) and IgG (Fig. 2c) was seen in parenchyma at or around the injured sites of all electrode-implanted animals. Immunofluorescence quantification confirmed FMT results and significant differences for both albumin (Fig. 2d,e) and IgG (Fig. 2f) extravasation were observed, wherein Michigan electrodes exhibited a significantly higher breach in comparison to microwire electrodes ($p < 0.01$) at 16WPI.

Supplementary data related to this article can be found online at http://dx.doi.org/10.1016/j.biomaterials.2013.03.007.

3.2. Influence of BBB breach on electrode failure

In order to elucidate the effects of BBB breach on intracortical electrode function, we implanted adult rats with two widely used intracortical electrode arrays in the rat barrel cortex. Evoked potentials obtained upon whisker stimulation [19] were recorded once a week for a period of 16WPI. The evoked recordings were filtered and sorted for action potential spikes (Fig. 3a) and signal-to-noise ratios (SNRs) were calculated. Results from the electrophysiological evoked recordings showed that the Michigan electrodes, which also exhibited a significantly higher BBB breach, failed to record within a period of 10 days (Fig. 3b) when compared to microwire electrodes, which provided stable recordings for a period of up to 84 days (Fig. 3b). The microwire electrodes also induced a significantly lower breach of the BBB. It is relevant to note that the commercially available microwire electrodes used in this study have a ~200% larger physical imprint in terms of volume of brain tissue displaced *in vivo* compared to the Michigan electrodes.

3.3. Wound healing response across electrode types

In order to determine if the electrodes exhibited differential wound healing and BBB stabilization responses, we determined, using quantitative real time polymerase chain reaction (qRT-PCR)

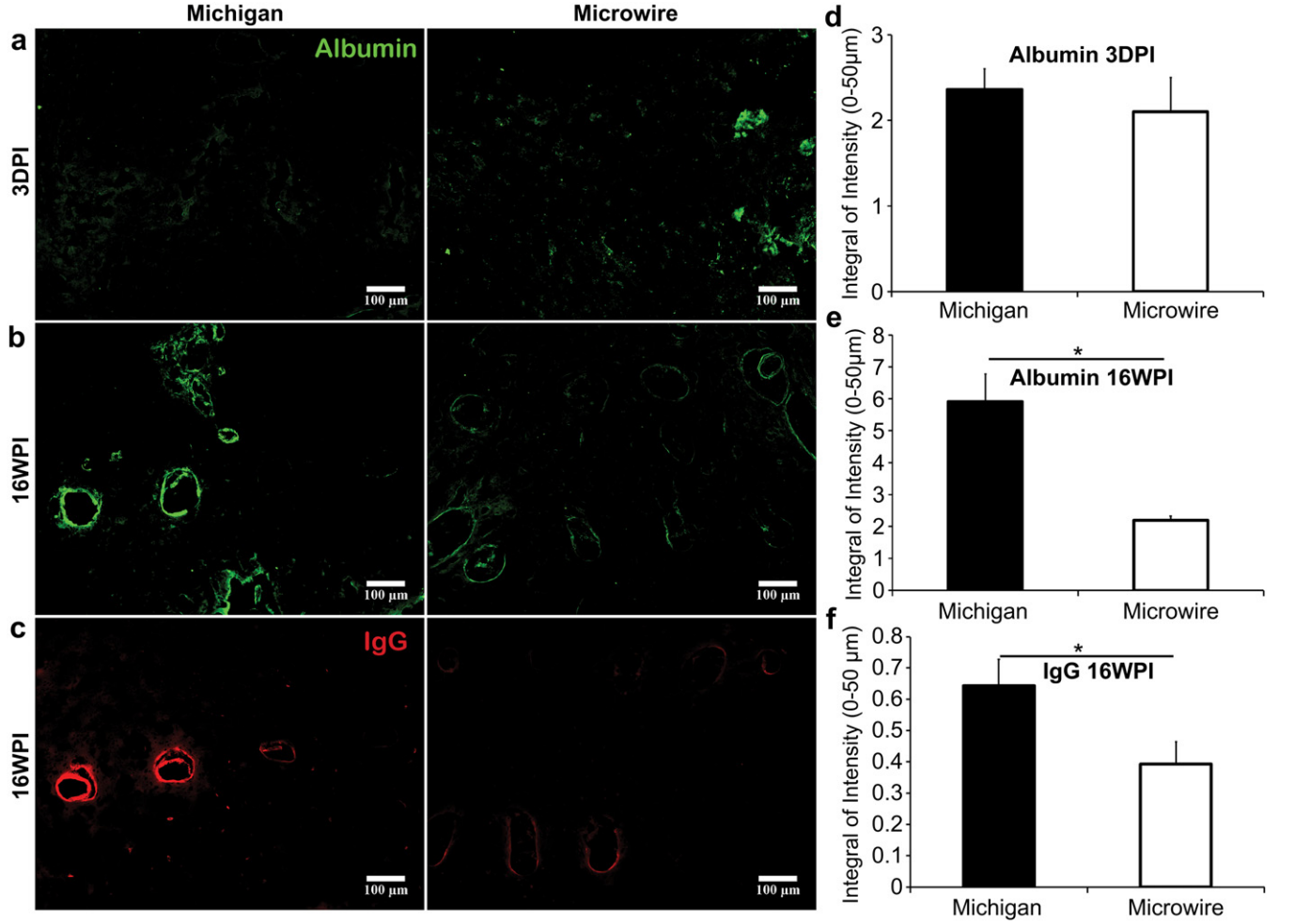

Fig. 2. Immunohistological assessment of BBB breach. (a) and (b) Representative immunohistochemical stains against extravasated albumin at 3DPI and 16WPI respectively. This is quantified in (d) and (e) respectively. (c) Representative micrograph of IgG immunoreactivity at 16WPI which is quantified in (f). Scale bars are 100 μm. Values are represented as mean ± s.e.m ($n = 6$/group).

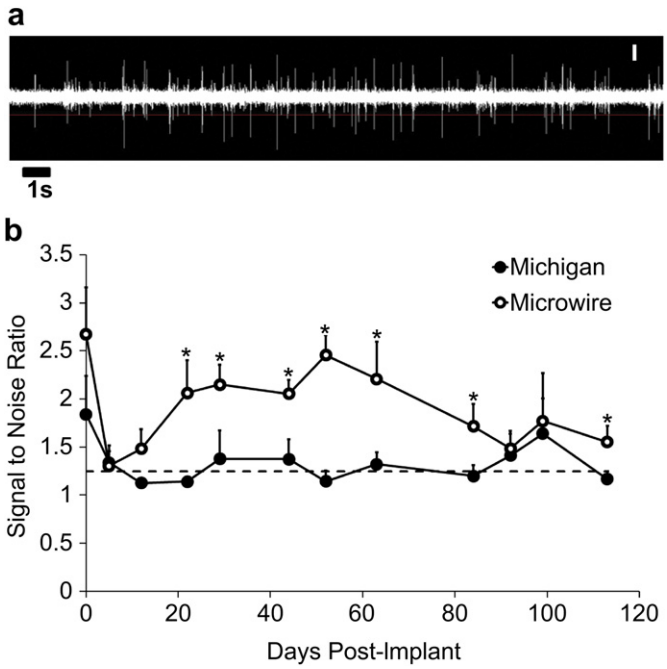

Fig. 3. Electrophysiological performance of intra-cortical electrodes. (a) Representative evoked spikes during a recording session, the SNRs of which are computed. (b) SNRs of Michigan (filled circles) and microwire (open circles) electrodes over a period of 16 weeks. The dotted line indicates SNR value below which data are considered noise. Values are represented as mean ± s.e.m ($n = 4$/group).

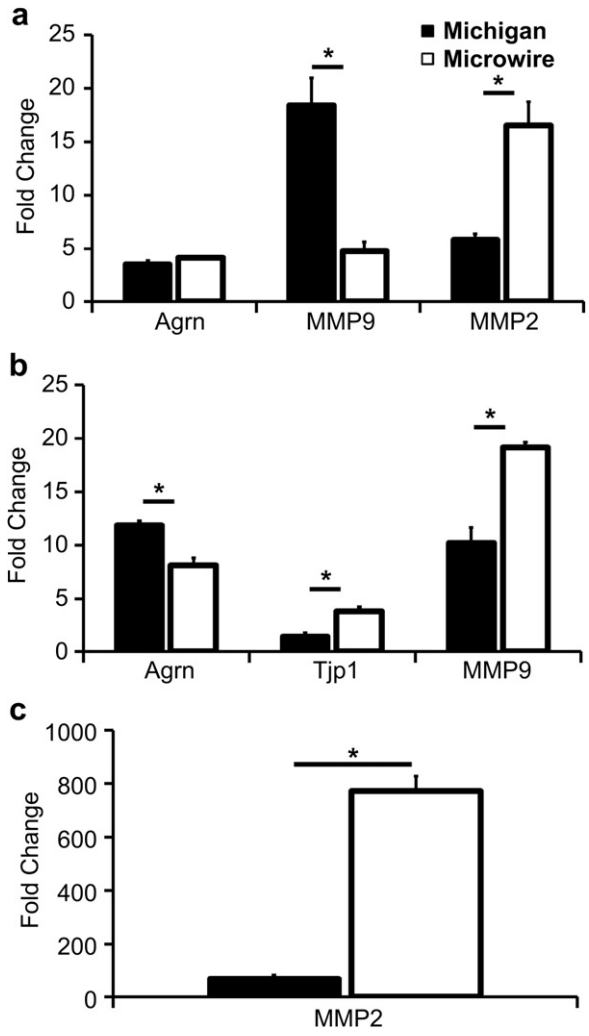

Fig. 4. qRT-PCR analysis of BBB proteins (agrin [Agrn], and tight junction protein [Tjp1]) and MMPs -2 and -9 around Michigan (black bars) and microwire (white bars) electrode implant sites. (a) Fold changes in gene regulation at 3DPI. (b) Fold changes in gene regulation at 16WPI. (c) Fold change in gene regulation of MMP2 at 16WPI. Values are represented as mean ± s.d. ($n = 3$/group).

analysis,the regulation of matrix metalloproteinase (MMP)-2 (known to promote wound healing) [20], MMP-9 (known to exacerbate BBB permeability and inflammation) [21,22], and proteins that stabilize the BBB: tight junction proteins (tjp-1 also known as ZO-1), agrin, and claudin [8] (Fig. 4). Fold-changes in gene expression were calculated with respect to control (uninjured, naive) animals. A three-fold or higher change in gene expression was considered significant [11]. An analysis of MMP-9 expression showed a significant difference between electrodes at 3DPI (Fig. 4a, microwire electrodes ~5 fold, Michigan electrodes ~18 fold, $p < 0.05$) but at 16WPI (Fig. 4b), microwire electrodes (~19 fold) showed a significantly higher ($p < 0.05$) expression of MMP-9 in comparison with Michigan electrodes (~10 fold). Analysis of the wound healing marker MMP-2 showed that microwire electrodes had a significantly enhanced wound healing response acutely (3DPI, Fig. 4a, ~17 fold, $p < 0.05$) and chronically (16WPI, Fig. 4c, ~772 fold, $p < 0.05$), when compared with Michigan electrodes. Since MMP-2 is associated with wound healing and angiogenesis [20,23], we quantified the collagen IV positive blood vessels [21] around electrode implant sites and found that microwire electrodes had a significantly ($p < 0.05$) higher blood vessel density in comparison with Michigan electrodes (Fig. S2 a–d). Agrin ($p < 0.05$), a protein found in the basal lamina of the BBB and important for BBB integrity, was also upregulated at both 3DPI (Fig. 4a) and 16WPI (Fig. 4b) when compared to controls for both Michigan and microwire electrodes. No significant differences in agrin gene regulation were noted at 3DPI between electrodes, but at 16WPI, Michigan (Fig. 4b) electrodes had a significantly ($p < 0.01$) higher expression of agrin in comparison with microwire electrodes. Tight junction protein gene tjp-1, which is important for the maintenance of BBB integrity, was significantly upregulated at 16WPI for microwire electrodes (Fig. 4b, ~4 fold). Overall, these data, using multiple indicators of BBB stability, corroborate the FMT imaging data demonstrating that microwire electrodes elicit a strong and significant wound healing response leading to relatively better BBB repair, whereas the Michigan electrodes elicit a disrupted BBB state.

3.4. Immunohistochemistry to detect infiltration of myeloid cells and chronic neurodegeneration around electrode sites

In order to understand the consequences of a breached BBB and its effects on chronic electrode function, we used immunohistochemistry to probe brain tissue sections for presence of $CD14^+$ monocytes, $CD4^+$ T-cells (MHC-II), $CD8a^+$ T-cells (MHC-I), mast cells, $CD32^+$ and $CD86^+$ macrophages, and ninjurin, which is a protein expressed on monocytes and mediates the transmigration of peripheral blood cells into the central nervous system (CNS) [24]. We observed that at 3DPI, $CD68^+$microglia and $GFAP^+$ astrocytes were the major cell types present at the electrode–cortex interface (Fig. 5). However, at 16WPI, the $GFAP^+$ and $CD68^+$ glial reaction was reduced in comparison with 3DPI, and was localized to the implant sites (Fig. 5). At 16WPI, implants had persistent presence of infiltrating myeloid cells as indicated by the positive staining for $CD4^+$ and $CD8a^+$ T-cells, $CD14^+$ monocytes, mast cells and ninjurin (Fig. 6). Animals implanted with Michigan intracortical electrodes

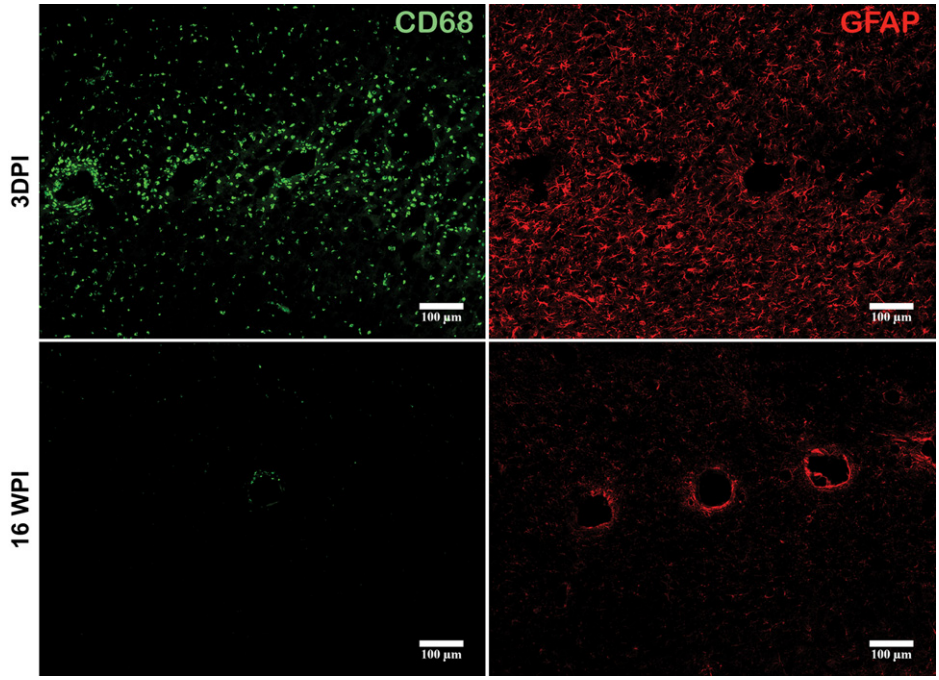

Fig. 5. Immunohistological assessment of glial cell activation. Representative micrographs depicting the temporal change in the presence of reactive astrocytes ($GFAP^+$) and macrophages ($CD68^+$) around Michigan electrodes at 3 DPI and 16WPI. Scale bars are 100 μm.

showed an increased presence of memory $CD4^+$ and $CD8a^+$ effector T-cells, $CD14^+$ monocytes, ninjurin expressing monocytes, and mast cells when compared to microwire electrodes (Fig. 6). These data suggest that myeloid cells invade the implant site, are present chronically, and mediate inflammation. At 16WPI, brain tissue from animals implanted with Michigan and microwire electrodes also showed the presence of $CD32^+$ and $CD86^+$ cells (Fig. S3) indicating the presence of pro-inflammatory macrophages around these intracortical electrode implants [25,26]. Overall, the presence of pro-inflammatory macrophages and myeloid cells was heightened in intracortical electrode implanted animals when compared to naïve controls. Since BBB breach is implicated in neurodegeneration [27] and a loss of recording may result from inflammation induced neuronal dysfunction in the vicinity of the electrodes, we used antibodies against paired helical filaments (PHF) and AT-8 [12] to investigate neurodegeneration in the vicinity of the electrodes. Tissue from both electrode implant groups showed positive immunoreactivity for PHF and AT-8 (Fig. S4) confirming active neurodegeneration around electrode implant sites.

3.5. Intraelectrode performance variability and BBB breach

As Michigan and microwire have different physical features, we wanted to explore if performance differences between electrodes of the same physical design could also be correlated to BBB state differences. In order to do this, we chose two animals from the microwire implantation group: microwire animal number 3 (MWA3) that displayed relatively poor SNRs over time and microwire animal number 5 (MWA5) that displayed higher and steady SNRs over time (Fig. 7a,b). High immunoreactivity for rat serum IgG was found in areas circumscribing the electrode shanks in MWA3 (Fig. 7c). Upon staining for neurons (NeuN), very few neurons were found around shank sites in MWA3, in contrast with MWA5 (Fig. 7d). To assess if there was a difference in the expression of genes encoding for cytokines (neurotoxic [interleukin (IL) - 1β, IL6, IL1Ra, and TNFα], or myeloid cell regulators [IL12β, IL17α, and TNFsF13b]), we performed qRT-PCR assays on tissue collected from IgG positive areas from both animals (Fig. S5). The transcripts for IL1β and IL6, and TNFα (pro-inflammatory cytokines known to exacerbate BBB permeability and neurotoxicity [8,28–32]) were significantly higher for MWA3 (Table 1) when compared with MWA5. Conversely, the IL-1 receptor agonist (IL1Ra, antagonizes IL-1b signaling and promotes neuroprotection [11,33,34]) was higher for MWA5. Interleukin 12B (IL12B), TNF super-family 13B (TNFsF13B), and IL17α had significantly higher transcript levels for MWA3 (Table 1). These cytokines are highly expressed in severe chronic neuroinflammatory diseases such as multiple sclerosis, and are potent B and T-cell activators [11,35–37]. Overall, these data establish that in a subset of animals where the same electrode type was implanted and yet showed a differential intraelectrode functional response, differential BBB breach and cytokine transcript level regulation correlate well to electrophysiological performance. Specifically, the electrodes that showed a stable functional response had a less permeable BBB and lower transcript levels of cytokines that exacerbate BBB permeability and neuroinflammation.

4. Discussion

The success of a chronically functional, reliable BCI relies on the ability to implant and integrate with brain tissue. While significant research has gone into engineering synthetic materials and devices, tissue integration is still difficult for a number of reasons such as material incompatibility, adverse foreign body responses, implant associated trauma, and biofouling at the device- brain tissue interface. The field of BCI is nascent, and the long-term success of any of these clinical interventions is completely reliant on reliable interfacing and mitigating deleterious tissue responses. Surprisingly, for BCIs, there has been little or no research to uncover the mechanistic link between the physiological response and intracortical electrode failure. To address this, we investigated the acute and chronic consequences of BBB disruption and its effects on intracortical recording electrode function. We demonstrate that electrodes that fail chronically have a highly permeable BBB leading to an increased presence of active inflammatory cells and

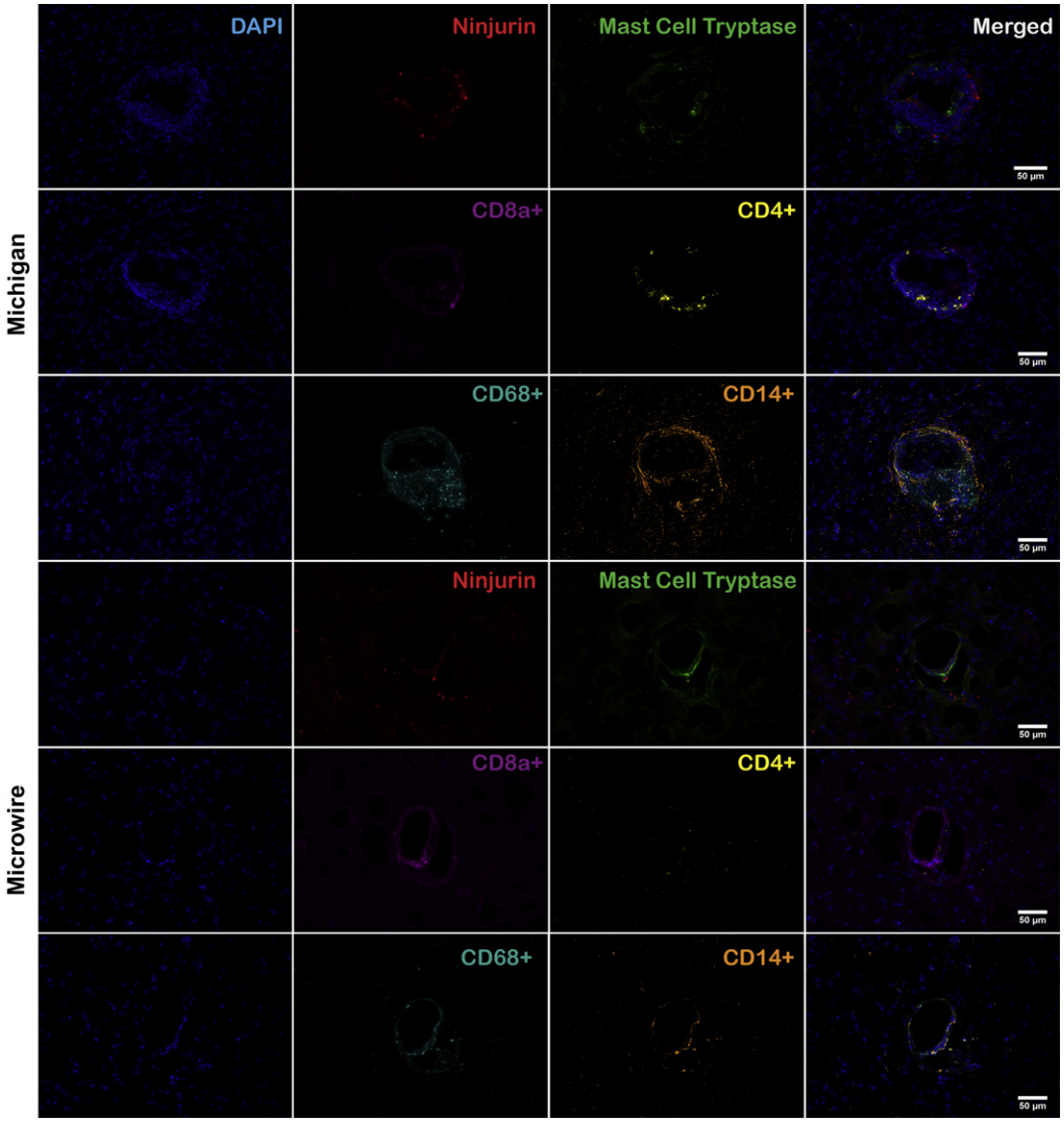

Fig. 6. Immunohistological assessment of myeloid cell infiltration. This representative figure shows the presence of ninjurin expressing monocytes, mast cells, $CD68^+$ microglia, $CD14^+$ monocytes, and $CD8a^+$ and $CD4^+$ T-cells around Michigan and microwire implants at the end of 16WPI. Scale bars are 50 μm.

neurotoxic factors, whereas electrodes that perform better have significantly better healing of the wound and a lower BBB breach. Our data suggest that intracortical electrodes induce a chronic breach of the BBB which, in a positive feedback loop, leads to chronic inflammation, culminating in neurodegeneration and electrode failure (Fig. 8).

The metallic components associated with commercially available intracortical electrode implants are incompatible with conventional non-invasive imaging techniques such as computed tomography (CT) and magnetic resonance imaging (MRI) (Fig. S6 a–c). Fluorescence molecular tomography (FMT) is a powerful preclinical tool that allows quantitative 3-D deep tissue fluorescence imaging [38] owing to the use of fluorophores that have excitation/emission profiles in the near-infrared (NIR) wavelength. The FMT technique has been successfully used previously to image other brain pathologies [39,40]. In this study, we adapted the FMT-NIR imaging technique to non-invasively image the state of the BBB using an albumin-Cy7 conjugate [17]. Using non-invasive FMT imaging, we were able to quantitatively differentiate between the extent of BBB breach in animals implanted with Michigan and microwire electrodes at chronic time points, wherein Michigan electrodes showed a significantly higher breach in comparison with microwire electrodes. Others have reported a permeable BBB at chronic time points, based on measurements from *ex vivo* tissue [10,25,41–43]. Recently, Liu et al. have demonstrated increased BBB permeability and structural changes to vasculature detectable for up to at least 330 days post a deep brain stimulation electrode implant in humans [10]. An open BBB leads to the influx of various neurotoxic serum proteins [21,44], pro-inflammatory cells, and modulates expression of cytokines that can lead to neurodegeneration and cell death [8,10,25,27,28,45–47]. Indeed, in neurodegenerative disorders such as multiple-sclerosis and Alzheimer's disease, a highly permeable BBB contributes actively to the disease pathology and active neurodegeneration [27]. Therefore, BBB permeability is a critical factor that can predict electrode performance, and the non-invasive monitoring of the BBB can help facilitate chronic electrode function via means that can modulate BBB permeability.

Wound healing has been reported to take place after penetrating injuries to the CNS. However, little is known about the sequence of wound healing events around intracortical brain–electrode implants. Persistent micromotion of implanted

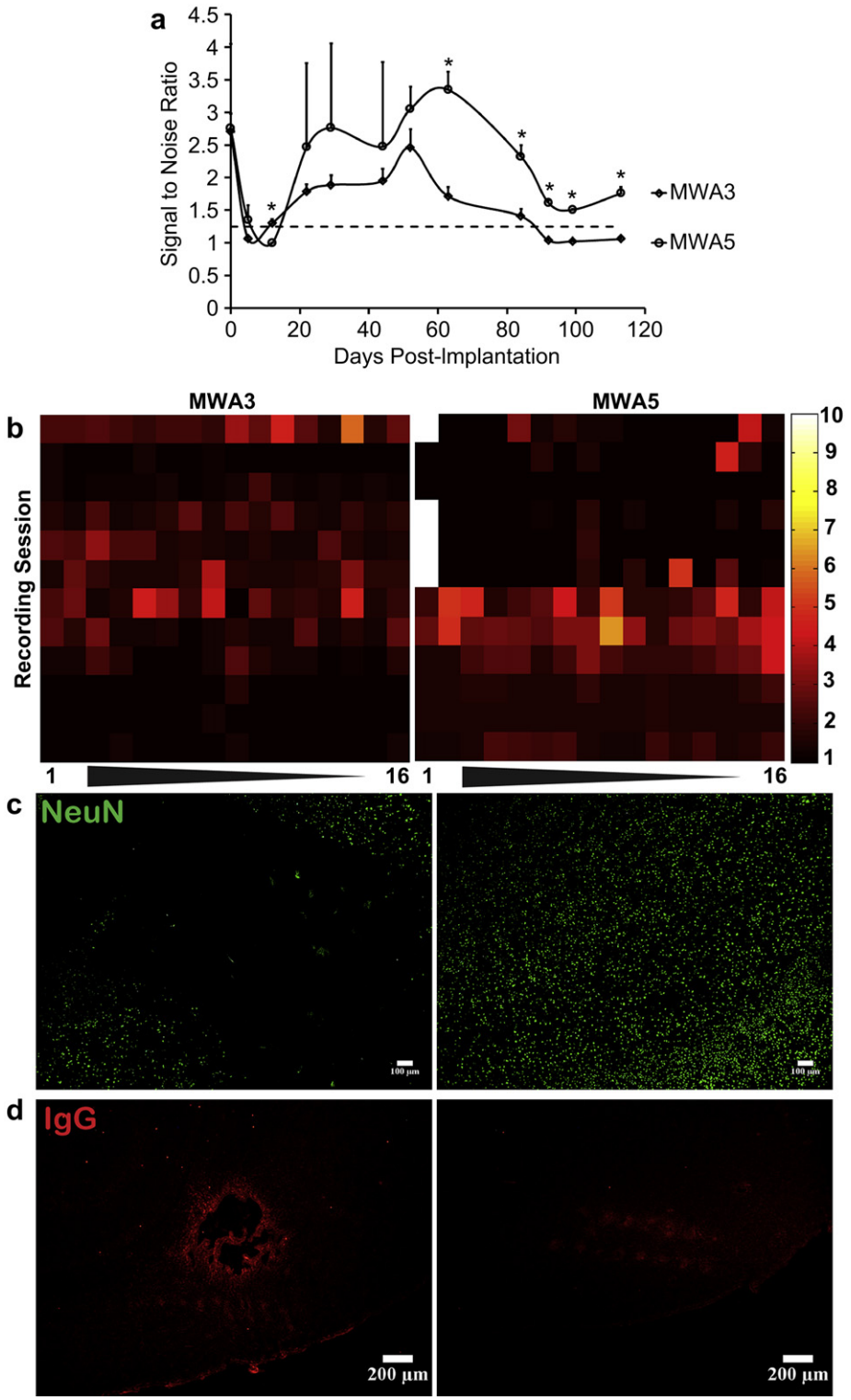

Fig. 7. Intraelectrode comparison of electrophysiological performance in microwire electrodes. (a) SNRs of MWA3 (open diamonds) and MWA5 (open circles) electrodes over a period of 16 weeks. Values are represented as mean ± s.e.m. (b) Heatmap representation of the SNRs of all 16 channels (abscissa) over each recording session (ordinate). Note that both heatmaps are on the same scale. The scale has been terminated at a value of 10 to clearly represent individual channel SNRs. (c) Representative fluorescent micrograph of live neurons (NeuN immunoreactivity) around MWA3 and MWA5 electrodes. (d) Representative micrograph of rat serum IgG immunoreactivity around MWA3 and MWA5 electrodes. Scale bars are 100 µm for (c) and 200 µm for (d).

intracortical electrodes could trigger a rather complex cascade of events [11,48] when compared to a single traumatic brain injury. In our studies, the elevated MMP-9 levels in tissue surrounding both electrodes may partly explain an open BBB at chronic times [21–23,27]. However, animals implanted with microwire electrodes exhibited a differential and significant wound healing response acutely and chronically, as indicated by the significant upregulation of tjp-1 and MMP-2 transcripts. MMP-2 has been

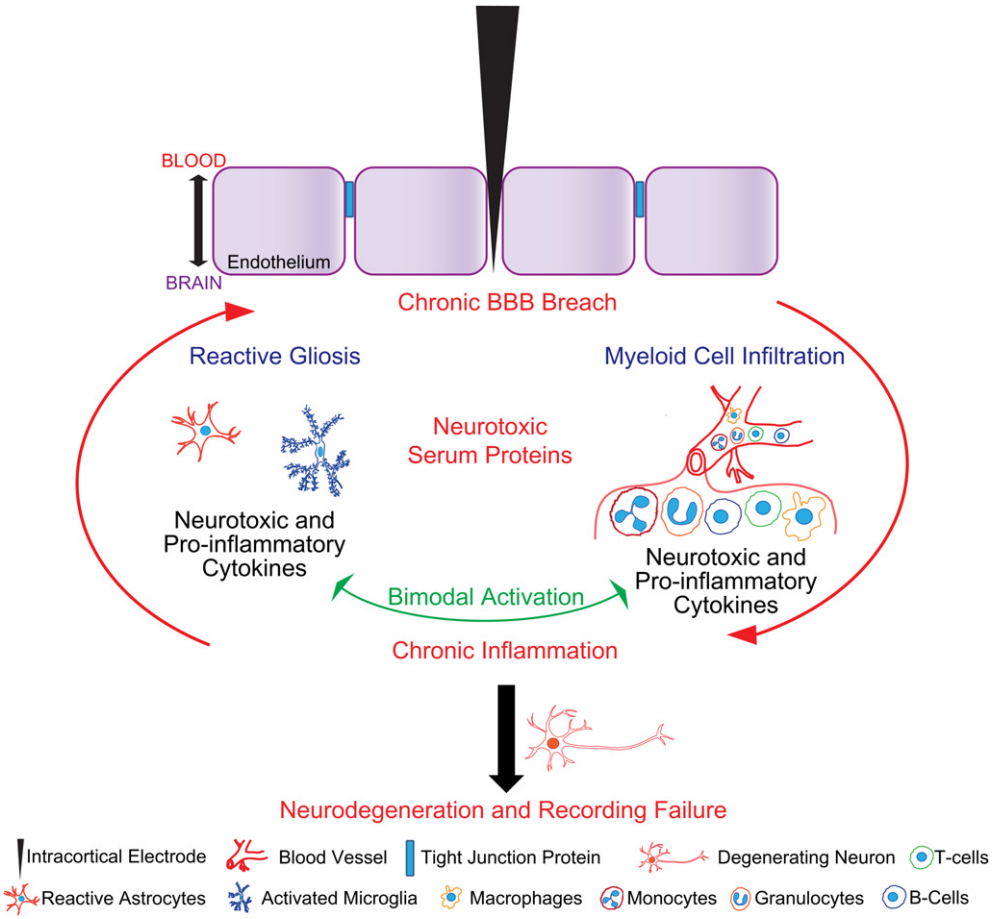

Fig. 8. Schematic illustration and the working model of chronic electrode failure. Intracortical electrodes induce a chronic BBB breach, which leads to the extravasation of neurotoxic serum proteins, and an infiltration of myeloid cells. Reactive gliosis and myeloid cell activation occurs in a bimodal manner, leading to the production of neurotoxic and proinflammatory cytokines. These cytokines increase BBB permeability, and cause chronic inflammation resulting in a positive feedback loop, that leads to neurodegeneration and loss of chronic electrode function.

reported to facilitate wound healing and promote neuronal regeneration after spinal cord injury [20,23]. Additionally, MMP-2 can attenuate inflammation by cleaving chemokines such as monocyte chemoattractant protein (MCP)-3 to terminate the chemotaxis of inflammatory cells, proteolytically degrade axon growth inhibitory chondroitin sulfate proteoglycans, and augment wound repair by angiogenesis [11,20]. Therefore, the upregulation of MMP-2 in microwire electrodes, in corroboration with BBB stabilizing proteins, possibly indicates enhanced stability and reduced micromotion when compared to Michigan electrodes, ultimately resulting in better chronic electrode function.

Myeloid cells are critical effectors and regulators of inflammation. The presence of these cells leads to the upregulation of various pro-inflammatory cytokines that modulate BBB permeability and lead to a sustained inflammatory response [49,50]. Histological analysis of tissue surrounding implanted electrodes indicates a more localized glial reaction around chronic electrode implants when compared to acute time points. These results point to a constantly evolving immune response to intracortical electrode implants, beginning with robust and widespread reactive gliosis acutely, which eventually diminishes and is accompanied by the heightened presence of various myeloid cells chronically. Therefore, myeloid cells present around intracortical electrode implants likely interact with reactive glia leading to a sustained inflammatory response and loss of chronic electrode function. Pro-inflammatory $CD32^+$ and $CD86^+$ B-cells and macrophages are known activators of T-cell proliferation [32]. Intracortical electrode implants also induce the proliferation of memory $CD4^+$ and $CD8^+$ T-cells which are responsible for antigen recognition and induction of a sustained pro-inflammatory response [51]. Following extravasation into the CNS parenchyma, T-cells also interact with intrinsic CNS glial cells, and activate them. The activated glia in turn can express molecules that are associated with an ability to stimulate T-cells with antigens [52,53]. Upon activation, microglia and astrocytes can produce numerous protein mediators, including cytokines (both pro-inflammatory and anti-inflammatory), growth factors, chemokines and neurotrophins [52,53]. Mast cells can also produce an array of mediators, such as pro-inflammatory cytokines (interleukin 1β (IL1β) and TNF-α), and growth factors. Activated mast cells also release chemoattractants that recruit eosinophils and monocytes, and also cause demyelination [54]. The lack of expression of neurotoxic cytokines and other pro-inflammatory cytokines such as IL1β, IL6, and TNF-α by stressed astrocytes and microglia reported previously [11], also indicates that these factors are likely produced by infiltrating myeloid cells. The chronic presence of these cells around electrode implant sites therefore highlights the importance of ascertaining the role of these myeloid cells alongside the contribution of reactive astrocytes and microglia in neuro-inflammation and neurotoxicity.

Various parameters such as the difference in electrode material type, electrode stiffness, and electrode design may have influenced the functional outcome of the particular electrode [7,42,55].

However, our results suggest that these parameters converge on affecting a critical biological factor, BBB permeability, which in turn determines electrode performance. Traditionally, microwire array electrodes (microwire in this study) outperform silicon based electrodes (Michigan in this study) which are unreliable for chronic recording applications [7,56]. Further, due to the differences in material properties and design, the electrodes may induce differential micromotion induced strains, that can be deleterious [48]. Karumbaiah et al. [11] have recently shown that primary CNS glia subjected to cyclic bi-axial strain upregulate a host of pro-inflammatory cytokines and MMPs that could have negative consequences for neuronal health. Indeed, embryonic day-18 (E18) primary neurons stretched in the presence of IL36Ra, an IL receptor antagonist found to be highly upregulated by strained astrocytes and microglia, showed a higher expression of apoptosis inducing factors when compared to E18 neurons stretched in the absence of IL36Ra. Previous studies have also shown that immune reactive cells recovered from around intracortical electrode implants secreted MCP-1 and TNFα [57], further suggesting that a sustained foreign body response around chronically implanted intracortical electrodes and presence of apoptosis inducing factors in the local milieu may lead to neuronal cell death.

The direct correlation of BBB permeability with electrode performance was further corroborated when differential intra-electrode performance was correlated to differential BBB breach when the electrode features were invariant. When two microwire implanted animals with differential recording performance were examined for BBB breach, the animal with the poorly performing electrode had significantly enhanced BBB permeability and lower neuronal viability. The animal further indicated increased transcript levels of neuroinflammatory cytokines belonging to the interleukin and TNF families. The proinflammatory cytokines IL6, IL1β and TNFα increase BBB permeability and are neurotoxic [8]. These cytokines can be released by activated astrocytes and act in a complex immunoregulatory loop [8,32,58]. The cytokines IL12β [59], IL17α [60], and TNFsF13B [36,37] have all been implicated in the activation of T-cells, B-cells, dendritic cells and macrophages. IL12β is expressed by activated macrophages that serve as an essential inducer of Th1 cells. IL12β has been found to be important for sustaining memory/effector Th1 cells [59]. IL17α is produced by activated T-cells and regulates the activities of nuclear transcription factor (NF kappa-B) and mitogen-activated protein kinases. IL17α can also stimulate the expression of IL6. IL17α also disrupts the BBB and increases BBB permeability by increasing oxidative stress [60].TNFSf13b is expressed by monocytes and glia and is a potent B-cell activator [36,37]. High levels of these cytokines are associated with several chronic inflammatory diseases and overexpression of these genes has been observed in the CNS of patients with neuroinflammatory disease [8,11,28,30–32,35–37,58]. These data confirm that chronic intracortical electrode function is in part determined by BBB permeability and inflammation that is mediated by a variety of myeloid cells.

Overall, our data indicate that Michigan electrodes, which failed faster relative to microwire electrodes in terms of their recording performance, had enhanced BBB permeability, infiltration of inflammatory myeloid cells, and a diminished wound healing response. This is in direct contrast with microwire microarray electrodes which had significantly lower BBB permeability, decreased inflammation, and an enhanced wound healing response.

5. Conclusions

In summary, we show that: (i) intracortical electrode implants lead to a chronically open BBB; (ii) we can non-invasively monitor BBB breach around electrode implant sites; (iii) there is a direct correlation of extent of BBB breach to electrode function; (iv) increased BBB permeability causes localized inflammation and infiltration of antigen presenting cells that further augment and mediate inflammation; and (v) microwire electrodes which showed superior functional ability over chronic time periods, had a significantly enhanced wound healing response. Therefore our data demonstrate that a chronically open BBB strongly correlates with electrode recording function and is a critical biological factor that could be monitored non-invasively. This finding informs future intracortical electrode designs which should ideally incorporate strategies to minimize BBB breach mediated neurotoxicity to enhance the duration of intracortical electrode performance.

Acknowledgments

We gratefully acknowledge Dr. Peter Davies and Albert Einstein College of Medicine for graciously gifting us the PHF-1 antibody. We thank Dr. Philip J. Santangelo for use of the Ziess Axiovert 200M and the Volocity image analysis software. We thank Dr. Edward Botchwey for access to the FMT. We thank Johannes Leisen for help with the MR imaging. This work was funded by the Defense Advanced Research Projects Agency (DARPA) MTO under the auspices of Dr. Jack Judy through the Space and NavalWarfare Systems Center, Pacific Grant/Contract No. N66001-11-1-4014.

Appendix ASupplementary data

Supplementary data related to this article can be found at http://dx.doi.org/10.1016/j.biomaterials.2013.03.007.

References

[1] Hochberg LR, Bacher D, Jarosiewicz B, Masse NY, Simeral JD, Vogel J, et al. Reach and grasp by people with tetraplegia using a neurally controlled robotic arm. Nature 2012;485:372–5.
[2] Kringelbach ML, Jenkinson N, Owen SL, Aziz TZ. Translational principles of deep brain stimulation. Nat Rev Neurosci 2007;8:623–35.
[3] Taylor DM, Tillery SIH, Schwartz AB. Direct cortical control of 3D neuroprosthetic devices. Science 2002;296:1829–32.
[4] Vetter RJ, Williams JC, Hetke JF, Nunamaker EA, Kipke DR. Chronic neural recording using silicon-substrate microelectrode arrays implanted in cerebral cortex. IEEE Trans Biomed Eng 2004;51:896–904.
[5] Schwartz AB, Cui XT, Weber DJ, Moran DW. Brain-controlled interfaces: movement restoration with neural prosthetics. Neuron 2006;52:205–20.
[6] Jackson A, Zimmermann JB. Neural interfaces for the brain and spinal cord-restoring motor function. Nat Rev Neurol 2012;8:690–9.
[7] Polikov VS, Tresco PA, Reichert WM. Response of brain tissue to chronically implanted neural electrodes. J Neurosci Methods 2005;148:1–18.
[8] Abbott NJ, Ronnback L, Hansson E. Astrocyte-endothelial interactions at the blood-brain barrier. Nat Rev Neurosci 2006;7:41–53.
[9] Kim YT, Hitchcock RW, Bridge MJ, Tresco PA. Chronic response of adult rat brain tissue to implants anchored to the skull. Biomaterials 2004;25:2229–37.
[10] Liu JY, Thom M, Catarino CB, Martinian L, Figarella-Branger D, Bartolomei F, et al. Neuropathology of the blood-brain barrier and pharmaco-resistance in human epilepsy. Brain 2012;135:3115–33.
[11] Karumbaiah L, Norman SE, Rajan NB, Anand S, Saxena T, Betancur M, et al. The upregulation of specific interleukin (IL) receptor antagonists and paradoxical enhancement of neuronal apoptosis due to electrode induced strain and brain micromotion. Biomaterials 2012;33:5983–96.
[12] McConnell GC, Rees HD, Levey AI, Gutekunst CA, Gross RE, Bellamkonda RV. Implanted neural electrodes cause chronic, local inflammation that is correlated with local neurodegeneration. J Neural Eng 2009;6:056003.
[13] Bradford MM. A rapid and sensitive method for the quantitation of microgram quantities of protein utilizing the principle of protein-dye binding. Anal Biochem 1976;72:248–54.
[14] Cornford EM, Hyman S. Blood-brain barrier permeability to small and large molecules. Adv Drug Deliv Rev 1999;36:145–63.
[15] Seiffert E, Dreier JP, Ivens S, Bechmann I, Tomkins O, Heinemann U, et al. Lasting blood-brain barrier disruption induces epileptic focus in the rat somatosensory cortex. J Neurosci 2004;24:7829–36.
[16] van Vliet EA, da Costa Araujo S, Redeker S, van Schaik R, Aronica E, Gorter JA. Blood-brain barrier leakage may lead to progression of temporal lobe epilepsy. Brain 2007;130:521–34.
[17] Klohs J, Steinbrink J, Bourayou R, Mueller S, Cordell R, Licha K, et al. Near-infrared fluorescence imaging with fluorescently labeled albumin: a novel

method for non-invasive optical imaging of blood-brain barrier impairment after focal cerebral ischemia in mice. J Neurosci Methods 2009;180:126–32.
[18] Hatashita S, Hoff JT. Brain edema and cerebrovascular permeability during cerebral ischemia in rats. Stroke 1990;21:582–8.
[19] Wang Q, Webber RM, Stanley GB. Thalamic synchrony and the adaptive gating of information flow to cortex. Nat Neurosci 2010;13:1534–41.
[20] Hsu JY, McKeon R, Goussev S, Werb Z, Lee JU, Trivedi A, et al. Matrix metalloproteinase-2 facilitates wound healing events that promote functional recovery after spinal cord injury. J Neurosci 2006;26:9841–50.
[21] Bell RD, Winkler EA, Singh I, Sagare AP, Deane R, Wu Z, et al. Apolipoprotein E controls cerebrovascular integrity via cyclophilin A. Nature 2012;485:512–6.
[22] Rosenberg G, Estrada E, Dencoff J. Matrix metalloproteinases and TIMPs are associated with blood-brain barrier opening after reperfusion in rat brain. Stroke 1998;29:2189–95.
[23] Zhang H, Adwanikar H, Werb Z, Noble-Haeusslein LJ. Matrix metalloproteinases and neurotrauma: evolving roles in injury and reparative processes. Neuroscientist 2010;16:156–70.
[24] Ifergan I, Kebir H, Terouz S, Alvarez JI, Lecuyer MA, Gendron S, et al. Role of Ninjurin-1 in the migration of myeloid cells to central nervous system inflammatory lesions. Ann Neurol 2011;70:751–63.
[25] Fitch MT, Silver J. Activated macrophages and the blood-brain barrier: inflammation after CNS injury leads to increases in putative inhibitory molecules. Exp Neurol 1997;148:587–603.
[26] Kigerl KA, Gensel JC, Ankeny DP, Alexander JK, Donnelly DJ, Popovich PG. Identification of two distinct macrophage subsets with divergent effects causing either neurotoxicity or regeneration in the injured mouse spinal cord. J Neurosci 2009;29:13435–44.
[27] Zlokovic BV. The blood-brain barrier in health and chronic neurodegenerative disorders. Neuron 2008;57:178–201.
[28] Banks WA. Blood-brain barrier transport of cytokines: a mechanism for neuropathology. Curr Pharm Des 2005;11:973–84.
[29] Banks WA, Erickson MA. The blood-brain barrier and immune function and dysfunction. Neurobiol Dis 2010;37:26–32.
[30] Deli MA, Descamps L, Dehouck MP, Cecchelli R, Joó F, Ábrahám CS, et al. Exposure of tumor necrosis factor-α to luminal membrane of bovine brain capillary endothelial cells cocultured with astrocytes induces a delayed increase of permeability and cytoplasmic stress fiber formation of actin. J Neurosci Res 2004;41:717–26.
[31] Didier N, Romero IA, Creminon C, Wijkhuisen A, Grassi J, Mabondzo A. Secretion of interleukin-1β by astrocytes mediates endothelin-1 and tumour necrosis factor-α effects on human brain microvascular endothelial cell permeability. J Neurochem 2004;86:246–54.
[32] Perry VH, Newman TA, Cunningham C. The impact of systemic infection on the progression of neurodegenerative disease. Nat Rev Neurosci 2003;4:103–12.
[33] Allan SM, Tyrrell PJ, Rothwell NJ. Interleukin-1 and neuronal injury. Nat Rev Immunol 2005;5:629–40.
[34] Loddick SA, Wong ML, Bongiorno PB, Gold PW, Licinio J, Rothwell NJ. Endogenous interleukin-1 receptor antagonist is neuroprotective. Biochem Biophys Res Commun 1997;234:211–5.
[35] Begovich AB, Chang M, Caillier SJ, Lew D, Catanese JJ, Wang J, et al. The autoimmune disease–associated IL12B and IL23R polymorphisms in multiple sclerosis. Hum Immunol 2007;68:934–7.
[36] Gandhi KS, McKay FC, Schsibeci SD, Arthur JW, Heard RN, Stewart GJ, et al. BAFF is a biological response marker to IFN-β treatment in multiple sclerosis. J Interferon Cytokine Res 2008;28:529–40.
[37] Thangarajh M, Gomes A, Masterman T, Hillert J, Hjelmström P. Expression of B-cell-activating factor of the TNF family (BAFF) and its receptors in multiple sclerosis. J Neuroimmunol 2004;152:183–90.
[38] Weissleder R. A clearer vision for in vivo imaging. Nat Biotechnol 2001;19:316–7.
[39] McCann CM, Waterman P, Figueiredo JL, Aikawa E, Weissleder R, Chen JW. Combined magnetic resonance and fluorescence imaging of the living mouse brain reveals glioma response to chemotherapy. Neuroimage 2009;45:360–9.
[40] Ntziachristos V, Tung CH, Bremer C, Weissleder R. Fluorescence molecular tomography resolves protease activity in vivo. Nat Med 2002;8:757–60.
[41] Potter KA, Buck AC, Self WK, Capadona JR. Stab injury and device implantation within the brain results in inversely multiphasic neuroinflammatory and neurodegenerative responses. J Neural Eng 2012;9:046020.
[42] Prasad A, Xue QS, Sankar V, Nishida T, Shaw G, Streit WJ, et al. Comprehensive characterization and failure modes of tungsten microwire arrays in chronic neural implants. J Neural Eng 2012;9:056015.
[43] Winslow BD, Christensen MB, Yang WK, Solzbacher F, Tresco PA. A comparison of the tissue response to chronically implanted Parylene-C-coated and uncoated planar silicon microelectrode arrays in rat cortex. Biomaterials 2010;31:9163–72.
[44] Davalos D, Ryu JK, Merlini M, Baeten KM, Le Moan N, Petersen MA, et al. Fibrinogen-induced perivascular microglial clustering is required for the development of axonal damage in neuroinflammation. Nat Commun 2012;3:1227.
[45] Gorter JA, Goncalves Pereira PM, van Vliet EA, Aronica E, Lopes da Silva FH, Lucassen PJ. Neuronal cell death in a rat model for mesial temporal lobe epilepsy is induced by the initial status epilepticus and not by later repeated spontaneous seizures. Epilepsia 2003;44:647–58.
[46] Hassel B, Iversen EG, Fonnum F. Neurotoxicity of albumin in vivo. Neurosci Lett 1994;167:29–32.
[47] Matz PG, Lewén A, Chan PH. Neuronal, but not microglial, accumulation of extravasated serum proteins after intracerebral hemolysate exposure is accompanied by cytochrome c release and DNA fragmentation. J Cereb Blood Flow Metab 2001;21:921–8.
[48] Gilletti A, Muthuswamy J. Brain micromotion around implants in the rodent somatosensory cortex. J Neural Eng 2006;3:189.
[49] Prinz M, Priller J, Sisodia SS, Ransohoff RM. Heterogeneity of CNS myeloid cells and their roles in neurodegeneration. Nat Neurosci 2011;13:1227–35.
[50] Ransohoff RM, Cardona AE. The myeloid cells of the central nervous system parenchyma. Nature 2010;468:253–62.
[51] Reinhardt RL, Khoruts A, Merica R, Zell T, Jenkins MK. Visualizing the generation of memory CD4 T cells in the whole body. Nature 2001;410:101–5.
[52] Aloisi F, Ria F, Adorini L. Regulation of T-cell responses by CNS antigen-presenting cells: different roles for microglia and astrocytes. Immunol Today 2000;21:141–7.
[53] Lehmann PV. The fate of T cells in the brain: veni, vidi, vici and veni, mori. Am J Pathol 1998;153:677–80.
[54] Skaper SD, Facci L. Mast cell-glia axis in neuroinflammation and therapeutic potential of the anandamide congener palmitoylethanolamide. Philos Trans R Soc Lond B Biol Sci 2012;367:3312–25.
[55] Harris JP, Capadona JR, Miller RH, Healy BC, Shanmuganathan K, Rowan SJ, et al. Mechanically adaptive intracortical implants improve the proximity of neuronal cell bodies. J Neural Eng 2011;8:066011.
[56] Liu X, McCreery DB, Carter RR, Bullara LA, Yuen TGH, Agnew WF. Stability of the interface between neural tissue and chronically implanted intracortical microelectrodes. IEEE Trans Rehabil Eng 1999;7:315–26.
[57] Biran R, Martin DC, Tresco PA. Neuronal cell loss accompanies the brain tissue response to chronically implanted silicon microelectrode arrays. Exp Neurol 2005;195:115–26.
[58] Schwaninger M, Sallmann S, Petersen N, Schneider A, Prinz S, Libermann TA, et al. Bradykinin induces Interleukin-6 expression in astrocytes through activation of nuclear Factor-κB. J Neurochem 2002;73:1461–6.
[59] Trinchieri G. Interleukin-12 and the regulation of innate resistance and adaptive immunity. Nat Rev Immunol 2003;3:133–46.
[60] Huppert J, Closhen D, Croxford A, White R, Kulig P, Pietrowski E, et al. Cellular mechanisms of IL-17-induced blood-brain barrier disruption. FASEB J 2010;24:1023–34.